International Journal of Nanomedicine

Dovepress
Taylor & Francis Group

Open Access Full Text Article

ORIGINAL RESEARCH

Prussian Blue Nanoparticle-Induced Alteration of the Polarization State of Tumor-Associated Macrophages as a Substantial Antitumor Mechanism Against Oral Squamous Cell Carcinoma (OSCC)

Zheng Zhang[1], Xiang Sun[2], Zihan Gao[1], Xin Lv[1], Hui Jia[1], Bin Huang[2], Chengwan Xia[1], Xudong Yang[1]

[1]Nanjing Stomatological Hospital, Affiliated Hospital of Medical School, Institute of Stomatology, Nanjing University, Nanjing, Jiangsu, People's Republic of China; [2]Key Laboratory for Bio-Electromagnetic Environment and Advanced Medical Theranostics, School of Biomedical Engineering and Informatics, Nanjing Medical University, Nanjing, Jiangsu, People's Republic of China

Correspondence: Xudong Yang; Chengwan Xia, Nanjing Stomatological Hospital, Affiliated Hospital of Medical School, Research Institute of Stomatology, Nanjing University, Nanjing, Jiangsu, People's Republic of China, Email yangxd66@163.com; 2665927917@qq.com

Introduction: Oral squamous cell carcinoma (OSCC) has a poor prognosis due to its immunosuppressive tumor microenvironment (TME), in which tumor-associated macrophages (TAMs) play a pivotal role in promoting disease progression and therapeutic resistance. This study examines whether Prussian blue nanoparticles (PB NPs) could reprogram TAMs and block tumor-stroma communication in OSCC.

Methods: PB NPs were synthesized using polyvinylpyrrolidone-assisted coprecipitation and characterized by transmission electron microscopy, dynamic light scattering, and UV-Vis spectroscopy. In vitro, their effects on macrophage polarization were assessed via immunofluorescence, Western blotting (CD206/CD86), and ELISA (TGF-β1/IL-6/TNF-α). The impact on OSCC-macrophage interaction was evaluated using CCK-8 assays, transwell co-culture systems with conditioned media. In vivo, xenograft-bearing mice were used to assess PB NP effects on OSCC-TAM crosstalk. Tumor growth, Ki67 proliferation index, and TAM phenotypes ($CD206^+$/$CD86^+$) were analyzed. Systemic biocompatibility was further assessed through CCK-8 in vitro and hematological profiling and histopathological examination in vivo.

Results: PB NPs (diameter 57.43 ± 22.25 nm; zeta potential −17.36mV) were successfully made and showed good biocompatibility in vitro and in vivo. In vitro, they shifted M2 TAMs toward anti-tumor M1 phenotypes, reducing CD206 and TGF-β1 while increasing CD86 and pro-inflammatory cytokines (IL-6, TNF-α). This change disrupted OSCC-TAM communication, limiting tumor growth and migration. In vivo, PB NPs reduced tumor volume, lowered the $Ki67^+$ cell ratio, and increased the intratumoral M1/M2 macrophage ratio.

Conclusion: Prussian blue nanoparticles effectively modulate the immunosuppressive TME in OSCC by shifting TAM polarization from the pro-tumor M2 phenotype to the anti-tumor M1 phenotype, thereby interrupting critical tumor-stroma interactions. Given their intrinsic immunomodulatory properties and favorable biosafety profile, PB NPs represent a promising and safe therapeutic strategy targeting the TME in OSCC.

Keywords: Prussian blue nanoparticles, tumor microenvironment, tumor-associated macrophages, oral squamous cell carcinoma

Introduction

Oral squamous cell carcinoma (OSCC) accounts for approximately 90% of all oral malignancies, with 377,713 new cases diagnosed worldwide in 2020.[1–3] Despite advancements in multimodal therapies, the 5-year survival rate remains below 60%, underscoring the urgent need for novel treatment strategies.[4–8] Emerging evidence identifies the tumor microenvironment (TME) as a key driver of therapeutic resistance and disease progression in OSCC.[9–13]

The OSCC TME constitutes a dynamic network comprising three key components: immune cells (including tumor-associated macrophages [TAMs], myeloid-derived suppressor cells, regulatory T cells, natural killer cells, and dendritic

Received: 17 March 2025
Accepted: 22 August 2025
Published: 31 August 2025

Graphical Abstract

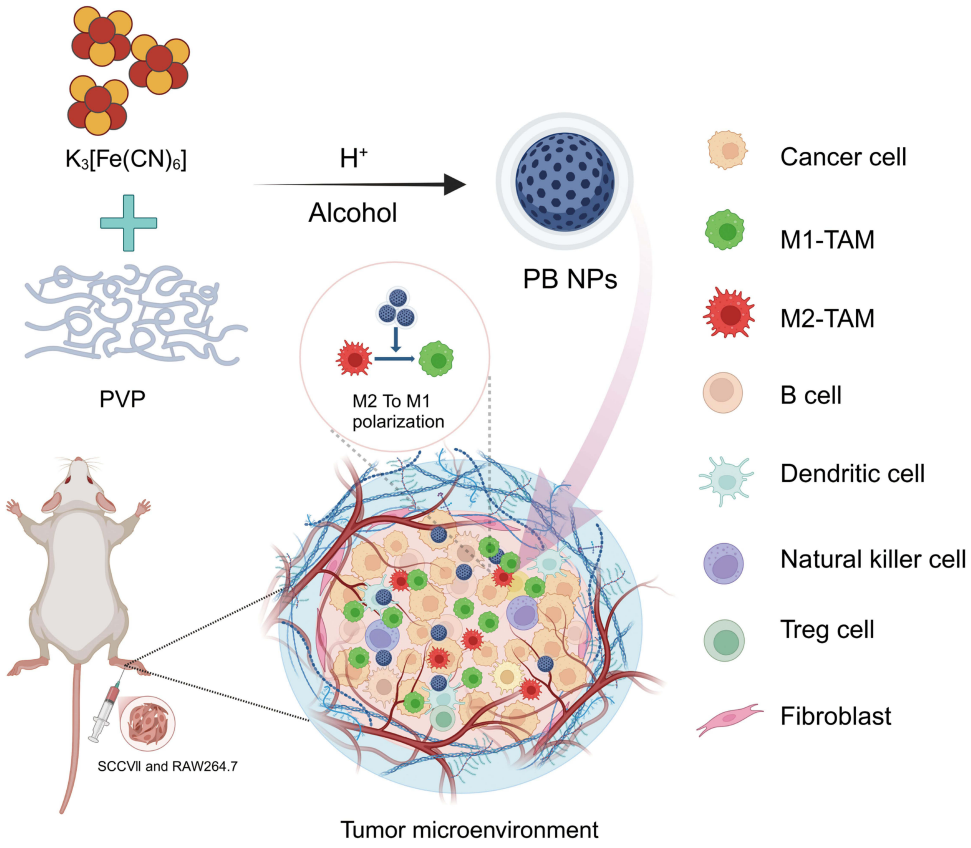

cells); stromal elements (predominantly cancer-associated fibroblasts); and extracellular mediators (such as cytokines, growth factors, the extracellular matrix, and exosomes).[14] This complex ecosystem not only supports tumor cell survival but also protects malignancies from chemotherapy and immunotherapy.[15] Although previous studies have elucidated the regulatory mechanisms involved in the tumor immune microenvironment, stromal cells, tumor angiogenesis, and cancer stem cells, the specific signaling pathway regulating the TME in head and neck squamous cell carcinoma (HNSCC) remains largely unknown. While previous studies have systematically characterized TME components, including immune cell subsets, stromal interactions, angiogenic mechanisms, and cancer stem cell niches,[16–19] our understanding of the specific signaling pathways governing TME remodeling in HNSCC remains limited.

Among the constituents of the TME, TAMs hold particular clinical significance owing to their functional plasticity.[20] Originating from peripheral blood monocytes, TAMs can exist in two distinct polarization states: pro-inflammatory M1 macrophages, which inhibit tumor growth, and immunosuppressive M2 macrophages, which promote tumor proliferation, metastasis, and drug resistance.[21,22] Notably, the balance between M1 and M2 polarization is dynamically reversible in response to microenvironmental cues,[23–25] highlighting the potential for therapeutic interventions that target macrophage phenotypes.

Prussian blue nanoparticles (PB NPs), constituted by the cyanide group (-C≡N-) bridges linking Fe(III) and Fe(II) ions and originating from the ancient pigment Prussian Blue first discovered in 1704 by Berlin artist Heinrich Diesbach, are an FDA-approved therapeutic platform whose clinical application stems from an FDA-approved antidote for thallium poisoning.[26–28]These nanoparticles exhibit multifunctional properties, including exceptional photothermal conversion efficiency, diagnostic imaging capabilities, enzyme-mimetic antioxidant activity, and drug delivery potential. Recent

advances have uncovered their ability to reprogram M2-polarized TAMs into tumor-suppressive M1 phenotypes.[26,29,30] However, this mechanism remains unexplored in OSCC despite its characteristically TAM-rich microenvironment.

Although emerging evidence indicates that PB NPs possess immunomodulatory potential by reprogramming M2-type macrophages into the M1 phenotype in certain malignancies, such as colon cancer,[31] this mechanism remains insufficiently investigated in oral squamous cell carcinoma (OSCC). OSCC is characterized by a highly immunosuppressive tumor microenvironment (TME) and a high infiltration of tumor-associated macrophages (TAMs).[32] Considering the pivotal role of M2-polarized TAMs in promoting tumor progression, metastasis, and therapeutic resistance, along with the limited efficacy of current treatment modalities, there is an urgent need to explore novel strategies capable of effectively modulating the OSCC TME—particularly those targeting TAM polarization. Therefore, this study aims to evaluate whether PB NPs can induce TAM polarization toward the M1 phenotype within the OSCC microenvironment and assess the associated therapeutic outcomes, thereby offering a promising immunotherapeutic approach for OSCC.

Materials and Methods

Synthesis and Characterization of PB NPs

The PB NPs were synthesized according to previous literature.[33] Polyvinylpyrrolidone K30 (PVP; 15 g) and potassium ferricyanide (0.55 g) were sonicated in 50 mL of ultrapure water to ensure homogeneous dispersion. The mixture was then magnetically stirred at 500 rpm for 30 min to achieve complete PVP hydration and salt dissolution. Subsequently, 150 mL of anhydrous ethanol was gradually introduced via a peristaltic pump under continuous stirring at 1,200 rpm, resulting in a homogeneous pale-yellow solution. The pH was adjusted to 2.0 ± 0.1 using 1 M hydrochloric acid. The reaction system was incubated in a water bath at 80°C for 3 h, followed by natural cooling to 25°C. Purification was performed through six cycles of ultrafiltration centrifugation (100 kDa MWCO, 1,000 ×*g*, 15 min) to remove residual solvents, unreacted precursors, and ionic byproducts ($[Fe(CN)_6]^{3-}$, K^+, CN^-, H^+, Cl^-). The resulting suspension was sterile-filtered using a 0.22-μm polyvinylidene fluoride (PVDF) membrane and lyophilized at −80°C under 0.05 mbar for 24 h, yielding PVP-PB NP powder.

Polyvinylpyrrolidone K30 and potassium ferricyanide were purchased from Aladdin Reagent (Shanghai, China). Absolute ethanol and hydrochloric acid were purchased from Sinopharm Chemical Reagent Co., LTD. (Shanghai, China) Ultrafiltration tubes were purchased from millipore (United States). The centrifuge used in this experiment was the Centrifuge 5430 model, manufactured by Eppendorf, Germany.

Morphological analysis was conducted using transmission electron microscopy (TEM; JEM-2100F, JEOL, Japan) at an accelerating voltage of 200 kV. UV–Vis–NIR absorption spectra (300–1,100 nm) were recorded using a Cary 5000 spectrophotometer (Agilent Technologies, USA). The hydrodynamic diameter and zeta potential were measured in triplicate using dynamic light scattering (DLS, ZetaSizer Nano ZS90, Malvern Panalytical, UK) under standardized conditions (25°C, 1 mM phosphate-buffered saline [PBS], pH 7.4).

Cell Culture

Human cell lines—including oral squamous cell carcinoma (OSCC) lines (HSC-3, HN-6, and CAL-27) and the normal human oral keratinocyte (HOK) cell line—along with murine SCC7 cells, were cultured in Dulbecco's Modified Eagle Medium (DMEM; Gibco, Thermo Fisher Scientific, USA) supplemented with 10% fetal bovine serum (FBS; Excell Bio, China) and 1% penicillin-streptomycin (Gibco, Thermo Fisher Scientific, USA). The cells were maintained in a humidified incubator at 37°C with 5% CO_2. The Raw 264.7 murine macrophage line was cultured under the same conditions but in an antibiotic-free medium. The culture medium was replenished every 48–72 h, and cells were subcultured at 80–90% confluence using 0.25% trypsin-EDTA (Gibco, Thermo Fisher Scientific, USA). All the cell lines were obtained from Fudan University (Shanghai, China).

Cell Counting Kit-8 (CCK-8) Cytotoxicity Assay

The cell viability of the HOK cell line was assessed using the CCK-8 assay with a detection kit (Beyotime Biotechnology, China). Cells were seeded in 96-well plates at a density of 8×10^3 cells/well and allowed to adhere for 24 h in complete DMEM under standard culture conditions. The medium was then replaced with fresh medium containing increasing concentrations of

PB NPs (0–25 μg/mL). After 24 h of exposure, the cells were washed twice with PBS (Gibco, Thermo Fisher Scientific, USA), followed by the addition of 10 μL of CCK-8 reagent per well. The plates were then incubated at 37°C for 2 h, after which absorbance was measured at 450 nm (with a reference wavelength of 650 nm) using an iMark microplate reader (Bio-Rad Inc., USA). Proliferation rates were calculated based on the absorbance values.

In vivo Biocompatibility

To evaluate the biocompatibility of PB NPs, we randomly assigned male Balb/c mice (6–8 weeks old, 20 ± 2 g) to two groups (n = 5) and received intravenous injections (100 μL/dose) every 3 days for 15 days. The control group received PBS, while the experimental group was administered PB NPs (10 mg/kg).[34] Body weight was monitored daily, and orbital blood samples were collected on day 16 for hematological analysis. The parameters measured included white blood cell (WBC) count, red blood cell (RBC) count, hemoglobin (HGB), hematocrit (HCT), platelet (PLT) count, mean corpuscular volume (MCV), mean corpuscular hemoglobin (MCH), mean corpuscular hemoglobin concentration (MCHC), red cell volume distribution width (RDW), mean platelet volume (MPV), lymphocyte percentage (Lymph %), monocyte percentage (Mono%), basophil percentage (Baso%), total bilirubin (TBIL), direct bilirubin (DBIL), total protein (TP), albumin (ALB), globulin (GLO), prealbumin (PA), alanine aminotransferase (ALT), aspartate aminotransferase (AST), alkaline phosphatase (ALP), gamma-glutamyl transpeptidase (GGT), adenosine deaminase (ADA), high-sensitivity C-reactive protein (CRP), UREA, creatinine (CREA), uric acid (URIC), β2-microglobulin (β2MG), glucose (GLU), and phosphorus (PHOS).[35] These analyses were conducted to evaluate the immune response and potential cytotoxic effects of PB NPs. To examine histological alterations in the organs of the mice, we harvested tumors and major organs (the heart, liver, spleen, lungs, and kidneys) from both untreated mice and those treated with PB NPs. The samples were fixed in 4% formalin, embedded in paraffin, sectioned into 4-μm-thick slices, and stained with hematoxylin and eosin (H&E). Representative images were captured using light microscopy (3DHISTECH, Hungary). The mice were obtained from the Comparative Medical Center of Yangzhou University.

Experiments Using Conditioned Medium

The conditioned medium for macrophages was prepared as follows: Initially, 5×10^6 HSC3, HN6, and CAL27 cells were seeded into 100 mm cell culture dishes (Corning, USA) and incubated for 24 h. Following incubation, the original medium was aspirated, and the cells were washed twice with PBS. The cells were then cultured in fresh DMEM for an additional 72 h. After this period, the supernatant was collected and centrifuged at 2,000 rpm for 40 min to remove cellular debris. The resulting supernatant was then mixed with fresh DMEM at a 1:1 ratio to produce conditioned medium 1 (CM1). To generate conditioned medium 2 (CM2) and conditioned medium 3 (CM3), we added PB NPs to CM1 at final concentrations of 5 and 10 μg/mL, respectively.

The conditioned medium for OSCC cells was prepared as follows: Raw 264.7 cells (2×10^5) were seeded into a six-well plate and incubated for 24 h. The original medium was then aspirated, and the cells were washed twice with PBS. Subsequently, the macrophages were cultured with CM1, CM2, or CM3 for an additional 48 h. The supernatant was collected and centrifuged at 2,000 rpm for 40 min to remove cellular debris. Finally, the supernatant was harvested and mixed with fresh DMEM at a 1:1 ratio to generate conditioned media CM4, CM5, and CM6, respectively.

Immunofluorescence Staining

The expression levels of CD86 and CD206 proteins in macrophages were assessed using immunofluorescence. Briefly, 1×10^5 macrophages were seeded onto glass-bottom confocal dishes. Following 24-h incubation, the culture medium was removed, and the cells were washed twice with PBS. Subsequently, the macrophages were exposed to fresh medium, CM1, CM2, or CM3 for an additional 48 h. The cells were then fixed with 4% paraformaldehyde for 30 min, permeabilized with 0.1% Triton X-100 for 10 min, and blocked with 3% bovine serum albumin (BSA) at room temperature for 30 min. Primary antibodies against CD86 (Proteintech, 13395-1-AP, China) and CD206 (Proteintech, 18704-1-AP, China) were applied and incubated overnight at 4°C. For detection, a DyLight 488-conjugated anti-rabbit IgG secondary antibody (Abcam, USA) was utilized. Nuclei were counterstained with DAPI (Beyotime Biotechnology, China) and visualized using confocal microscopy (Nikon Ti, Tokyo, Japan).

Western Blot Analysis

The protein expression levels of CD86 and CD206 in macrophages were evaluated via Western blot analysis. Macrophages treated with fresh medium, CM1, CM2, and CM3 were collected and lysed in RIPA buffer supplemented with 1 mM phenylmethylsulfonyl fluoride (PMSF) (Beyotime Biotechnology, China). The protein concentration of the lysates was quantified using a NanoDrop One spectrophotometer (Thermo Fisher Scientific, USA). Equal amounts of protein (5 μL/lane) from each sample were subjected to SDS-polyacrylamide gel electrophoresis and subsequently transferred onto a PVDF membrane (Immobilon, Millipore Corporation, Bedford, MA). The membranes were then blocked with Tris-buffered saline containing 5% (w/v) non-fat milk powder and 0.1% (v/v) Tween-20 before being incubated with primary antibodies against CD86 (Proteintech, 13395-1-AP, China) and CD206 (Proteintech, 18704-1-AP, China). Protein signals were detected using an ECL detection system (Amersham, Piscataway, NJ).

Enzyme-Linked Immunosorbent Assay (ELISA)

The cytokine profiles of macrophages exposed to fresh medium, CM1, CM2, and CM3 were evaluated using ELISA kits for IL-6, TNF-α, and TGF-β1, following the manufacturer's instructions. Specifically, 2×10^5 Raw 264.7 cells were seeded in six-well plates and incubated for 24 h. The initial culture medium was then replaced with fresh medium, CM1, CM2, or CM3. After an additional 48-h incubation, the supernatant was collected and centrifuged at 2,000 rpm for 15 min to remove cellular debris. For ELISA, standards (100 μL), samples (100 μL), and blanks were added to designated wells in microplates and incubated at 37°C for 90 min. Biotin-conjugated antibodies (100 μL) were subsequently added to the wells containing standards and samples, and the plates were sealed and incubated at 37°C for 1 h. Following five washes, streptavidin-HRP (100 μL) and substrate solution (100 μL) were added to each well and incubated at 37°C for 30 min and 15 min, respectively. Finally, stop solution (100 μL) was added to each well, and absorbance was measured at 450 nm within 15 min. The concentrations of IL-6, TNF- α, and TGF-β1 were determined using a standard curve.

Indirect Effects of PB NPs on the Proliferation of OSCC Cells Co-Cultured with Macrophages

To evaluate the indirect effects of PB NPs on the proliferation of OSCC cells, we established a coculture system of OSCC cells and macrophages using Transwell chambers (4 μm, Corning, USA). In the control group, 3×10^4 OSCC cells (HSC3, HN6, CAL27) were seeded in the lower chamber. For treatment group 1, 3×10^4 OSCC cells (HSC3, HN6, CAL27) were seeded in the lower chamber, while 5×10^3 Raw 264.7 cells were seeded in the upper chamber and incubated with fresh medium lacking PB NPs. For treatment group 2, 3×10^4 OSCC cells (HSC3, HN6, and CAL27) were seeded in the lower chamber, while 5×10^3 Raw 264.7 cells were seeded in the upper chamber and incubated with fresh medium containing 5 μg/mL PB NPs. For treatment group 3, 3×10^4 OSCC cells (HSC3, HN6, and CAL27) were seeded in the lower chamber, while 5×10^3 Raw 264.7 cells were seeded in the upper chamber and incubated with fresh medium containing 10 μg/mL PB NPs. After 48 h of coculture, the medium was aspirated, and OSCC cells were rinsed twice with PBS. Subsequently, 800 μL of CCK-8 reagent was added to each well, and the plates were incubated for an additional 2 h at 37°C. Absorbance at 450 nm was measured using an iMark microplate reader (Bio-Rad Inc., USA). Proliferation rates were calculated based on these absorbance readings.

Cell Wound Healing Assay

The cell wound healing assay was conducted to evaluate the indirect effects of PB NPs on the migration of OSCC cells. Specifically, OSCC cell lines (HSC3, HN6, and CAL27) were seeded into six-well plates and cultured until confluence exceeded 90%. A pipette tip was used to create a scratch perpendicular to the cell monolayer along a pre-marked line on the back of the plate. Following scratch formation, the cells were washed three times with sterile PBS to remove unattached cells, after which the medium was replaced with fresh medium and CM4/5/6. Phase-contrast images were captured immediately by microscopy (Nikon, Tokyo, Japan) after scratching and again 24 hours later.

Animal Study

After a 1-week acclimation period, male Balb/c mice (~20 g) were used to establish OSCC xenografts through subcutaneous implantation of murine SCC7 cells. For implantation, exponentially growing SCC7 cells were harvested, washed twice with sterile PBS (Gibco, Thermo Fisher Scientific, USA), and resuspended in ice-cold PBS at 1×10^6 cells/mL, followed by injection using a 30-gauge needle. Mice were randomly assigned to three experimental groups (n = 6 per group). Group 1 (Tumor Control) received a 100 μL subcutaneous injection containing 1×10^5 SCC7 cells in the right hind paw. Groups 2 and 3 received co-injections of 1×10^5 SCC7 cells mixed with 1×10^4 Raw 264.7 cells suspended in 100 μL PBS. Tumor development was monitored daily using digital calipers, with successful induction confirmed when tumor volume reached approximately 15 mm^3 within 7–10 days post-inoculation. Upon reaching this endpoint, peritumoral injections were initiated: Group 2 received 100 μL saline solution, Group 3 received 100 μL PB NPs suspended in saline at a concentration of 10 μg/mL, with injections administered every 3 days for a total of five doses. Group 1 served as the untreated control throughout the intervention period. Tumor volumes were measured daily and calculated using the formula $V = ½ ab^2$,[36] where a represents the tumor length and "b" the tumor width. Finally, the tumors were excised for further pathological examination. The animal experiments were carried out following the guidelines of the Nanjing Medical University Institutional Committee for the Care and Use of Laboratory Animals and were approved by the Committee on Ethical Use of Animals of Nanjing Medical University (Ethical code: IACUC-2406030).

Immunohistochemistry (IHC)

Protein expression levels of CD86, CD206, and Ki67 in murine tumor tissues were evaluated by IHC. Tumor specimens were first fixed in 4% formaldehyde and embedded in paraffin blocks. Subsequently, 4-μm-thick sections were prepared and subjected to a series of graded xylene and ethanol treatments. Antigen retrieval was performed by heating the sections in 10 mM citrate buffer (pH 6.0) using a microwave for 10 min. Endogenous peroxidase activity was quenched by incubating the sections with 0.3% hydrogen peroxide for 5 min. After blocking with 3% BSA for 1 h at room temperature, we incubated the sections overnight at 4°C with primary antibodies against CD86 (Affinity, DF6332, USA), CD206 (Proteintech, 18704-1-AP, China), and Ki67 (Proteintech, 28074-1-AP, China). The sections were then incubated with the MaxVision™ HRP-Polymer anti-Mouse/Rabbit IHC reagent (Kit-5020; Fuzhou Max Vision Biotechnology Development Co., Ltd., China) for 2 h at room temperature. Signals were visualized using 3,3′-diaminobenzidine (DAB) chromogen, followed by counterstaining with hematoxylin. Microscopic examination was performed using a light microscope (3DHISTECH, Hungary).

Immunohistochemical expression was quantified using the histochemistry score (H-Score) system, a semi-quantitative method that integrates staining intensity and the proportion of positively stained cells through the formula: H-Score =weakly stained cells (%) × 1 + moderately stained cells (%) × 2 + strongly stained cells (%) × 3, where staining intensity was graded as: 0 (negative, no staining), 1 (weak), 2 (moderate), or 3 (strong), with percentages representing the proportion of cells at each intensity level (summing to 100% per evaluated region), yielding a theoretical range of 0–300. For each tumor section, the scoring was performed on 5 randomly selected high-power fields (HPF) under a ×800 magnification.[37]

Statistical Analysis

Statistical analysis was performed using SPSS statistical software (version 23.0; IBM) and GraphPad Prism (version 9.5; GraphPad Software, La Jolla, CA, USA). Data are presented as means ± standard deviation. Comparisons among three or more groups were performed using one-way ANOVA. Repeated measures data were analyzed using MANOVA. Statistical significance is denoted as $*p < 0.05$, $**p < 0.01$, $***p < 0.001$, and $****P < 0.0001$. "ns" indicates no significant difference.

Results

Synthesis and Characterization of PB NPs

PB NPs were successfully synthesized, with hydrodynamic diameters of 57.43 ± 22.25 nm, as determined by dynamic light scattering (Figure 1A). TEM analysis revealed uniformly dispersed spherical nanoparticles (Figure 1B). The synthesized PB NPs exhibited a UV-Vis absorption peak at 693 nm. Notably, a slight shift toward longer wavelengths was observed in the UV-Vis spectrum when the solvent temperature increased from 4°C to 26°C (Figure 1C). The zeta

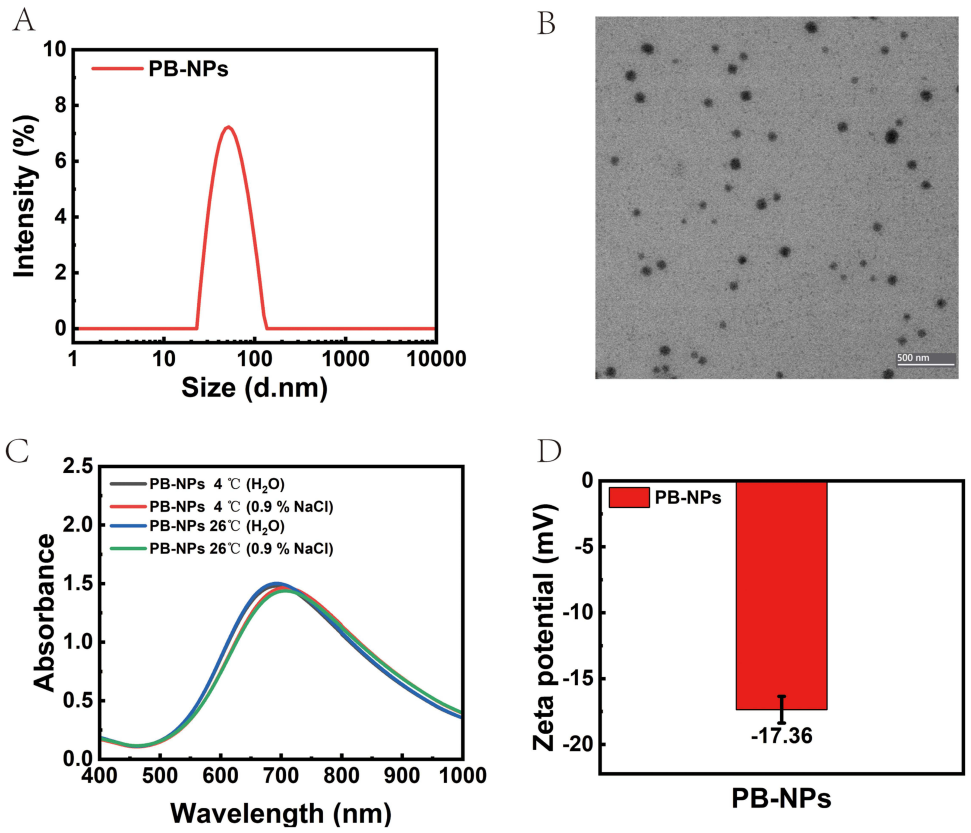

Figure 1 Characterization of PB NPs. Particle size distribution of PB NPs analyzed via DLS (**A**). Morphology of PB NPs assessed via TEM (**B**). UV-Vis absorption spectra of PB NPs. Scale bar: 500 nm.(**C**). Zeta potential of PB NPs (D).

potential of PB NPs was measured at −17.36 mV (Figure 1D). Taken together, these results demonstrate the excellent dispersibility and stability of PB NPs.

Biocompatibility of PB NPs

To evaluate the biological safety of PB NPs, we performed a CCK-8 assay in vitro. The results demonstrated that when HOK cells were incubated with a conditioned medium containing varying concentrations (0–25 μg/mL) of PB NPs for 24 h, no significant toxicity was observed at any concentration ($p > 0.05$), indicating high cytocompatibility (Figure 2A). To further assess the in vivo biosafety of PB NPs, we conducted an in vivo biosafety evaluation using Balb/c mice. As shown in Figure 2B, mice administered PB NPs exhibited no significant reduction in body weight compared to those in the normal saline injection group ($p > 0.05$). Additionally, hematological and histopathological analyses of major organs (the heart, liver, spleen, lung, and kidney) revealed no significant pathological changes ($p > 0.05$) in hematological parameters or major organ tissues (Figures 2C and D). Collectively, these findings demonstrate that PB NPs exhibit high biocompatibility both in vitro and in vivo, supporting their potential for safe biomedical applications.

In vitro Alteration of the Polarization State of TAMs

The TME is rich in TAMs, which constitute approximately half of the total tumor mass and predominantly exhibit an M2 phenotype.[38,39] Consequently, strategies targeting the inhibition or reprogramming of M2-type TAMs have emerged as pivotal and effective approaches in cancer therapy. To investigate the impact of PB NPs on macrophage polarization, we conducted a comprehensive set of experiments, including immunofluorescence staining, ELISA, and Western blot analysis. As illustrated in Figure 3A, M0 macrophages stimulated with tumor cell supernatant began to shift toward an M2 phenotype. Subsequently, these polarized M2 macrophages were exposed to varying concentrations of PB NPs. The results revealed a significant reduction in the M2 marker CD206, accompanied by a notable increase in the M1

https://doi.org/10.2147/IJN.S528763

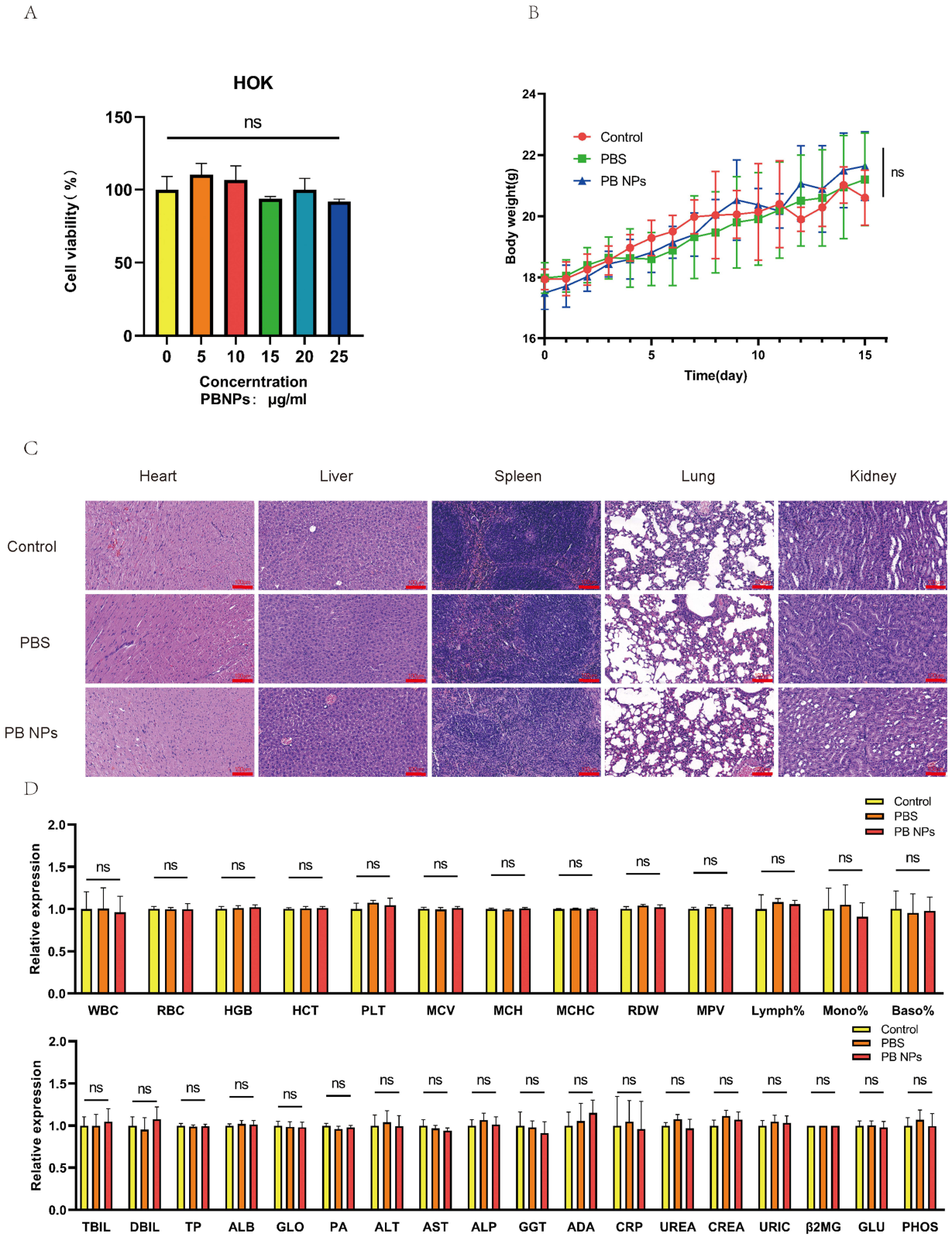

Figure 2 Biocompatibility of PB NPs. (**A**) Effect of different concentrations of PB NPs on HOK cell proliferation. (**B**) Body weight measurements before and after treatment with PB NPs or PBS. (**C**) H&E staining of five tissues (the heart, liver, spleen, lungs, and kidneys), Scale bar: 100 μm,(final magnification:×200). (**D**) Hematological parameters before and after treatment with PB NPs or PBS. "ns" indicates no significant difference.

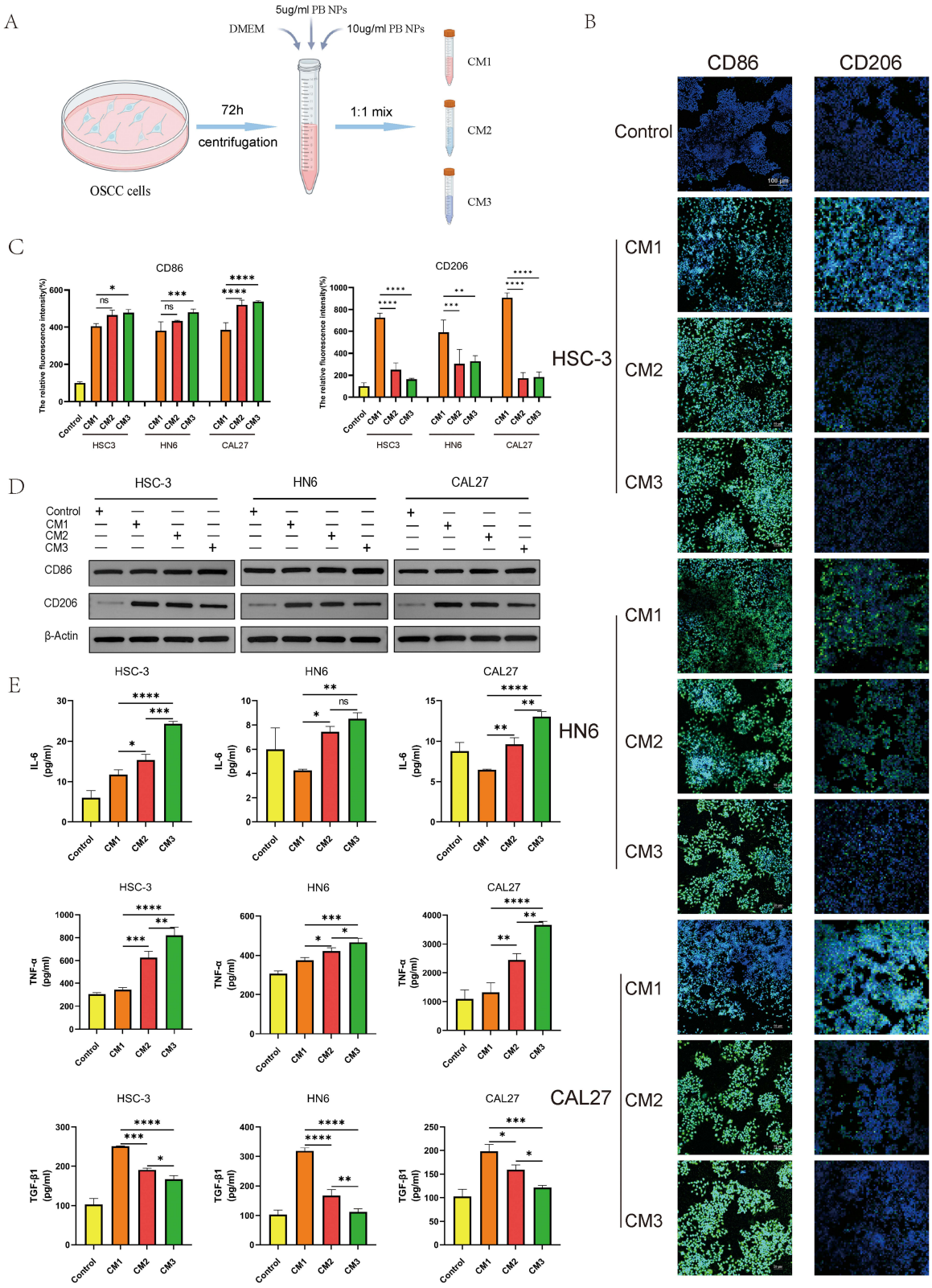

Figure 3 Alteration of the polarization state of TAMs induced by PB NPs in vitro. (**A**) Schematic illustration of the preparation processes for CM1, CM2, and CM3. (**B**) Immunofluorescence images showing CD86 or CD206 expression in TAMs treated with CM1, CM2, and CM3. (**C**) Relative fluorescence intensity of immunofluorescence signals. (**D**) Protein expression levels of CD86 and CD206 in TAMs treated with CM1, CM2, and CM3. (**E**) Protein expression levels of IL-6, TNF-α, and TGF-β1. *p < 0.05, **p < 0.01, ***p < 0.001, ****p < 0.0001; "ns" indicates no significant difference.

https://doi.org/10.2147/IJN.S528763

marker CD86. Immunofluorescence staining assays clearly demonstrated this shift ($p<0.05$) (Figure 3B, 3C), a trend that was further confirmed by Western blot analysis (Figure 3D). Furthermore, we can also observe that as the concentration of Prussian blue nanoparticles increases, the ratio of M1/M2 macrophages also shows an increasing trend. Macrophages in different polarization states exhibit distinct secretory profiles. M1-type macrophages secrete factors such as TGF-α and IL-6, while M2-type macrophages predominantly release TGF-β1. In this study, treatment with PB NPs altered the macrophage secretion profile, leading to increased secretion of TGF-α and IL-6 and decreased secretion of TGF-β1 ($p<0.05$) (Figure 3E). Similarly, analysis of the macrophage secretion profile revealed that increasing concentrations of PB NPs induced a significant upregulation of IL-6 and TNF-α—cytokines predominantly secreted by M1 macrophages—while simultaneously reducing the secretion of TGF-β1.These findings suggest that PB NPs have the potential to reprogram M2-type macrophages into M1-type macrophages, presenting a promising strategy for inhibiting tumor progression.

Disrupting the Communication Between OSCC and TAMs

M2 macrophages, also known as TAMs, have been shown to significantly enhance the proliferation and migration of OSCC cells. To investigate whether PB NPs can disrupt the interaction between OSCC cells and TAMs, we established a co-culture system utilizing Transwell chambers (Figure 4A). Results from the CCK-8 assay demonstrated that the presence of macrophages in the coculture environment promoted OSCC cell proliferation ($p<0.01$), whereas PB NPs reversed this effect ($p<0.05$) (Figure 4B). Additionally, conditioned media were prepared from macrophage supernatants treated with varying concentrations of PB NPs (Figure 4C). A scratch wound healing assay was then conducted to assess the influence of these conditioned media on the migratory capacity of OSCC cells. The results indicated that PB NPs effectively inhibited the promigratory effects of macrophages on OSCC cells. ($P < 0.001$)(Figures 4D and E).

To further confirm that PB NPs can block communication between OSCC cells and macrophages in vivo, we established an OSCC mouse xenograft tumor model. In the control group, only tumor cells were inoculated, whereas in the other two groups, both tumor cells and macrophages were inoculated. A total of 100 μL of either PBS or PB NPs was injected into the peritumoral area five times at 3-day intervals. Tumor volumes were calculated using the formula $V = 1/2\ ab^2$ (a: tumor length, b: tumor width). The presence of macrophages promoted tumor proliferation; however, treatment with PB NPs reversed this trend in vivo ($p<0.001$) (Figure 5A). These findings indicate that regulating macrophages through PB NPs is a feasible strategy for inhibiting OSCC progression.

The protein expression levels of CD86 and CD206 in macrophages were assessed via IHC to evaluate the polarization state of macrophages. Additionally, Ki-67 protein expression was measured to assess tumor cell proliferation. As shown in Figure 5B and C, treatment with PB NPs led to increased CD86 expression and decreased CD206 expression in macrophages, indicating a shift from M2 to M1 polarization ($p<0.001$). Additionally, Ki-67 protein expression in tumor cells was elevated following coculture with macrophages but was significantly reduced after PB NP treatment ($p<0.001$). These findings suggest that PB NPs inhibit the pro-proliferative effects of macrophages on OSCC cells by modulating macrophage polarization in vivo.

Discussion

The immunosuppressive TME, particularly M2-polarized TAMs, remains a major obstacle to effective immunotherapy in OSCC. Although immunotherapy has shown promise, its therapeutic efficacy is limited by TAM-mediated immune evasion and drug resistance mechanisms.[40,41] In this study, we developed PB NPs as novel TME modulators to address this challenge. Our experimental results demonstrated that PB NPs effectively reprogrammed M2 macrophages into tumor-suppressive M1 phenotypes, as evidenced by the downregulation of CD206, upregulation of CD86, and reversal of the cytokine secretion profile. This polarization shift disrupted OSCC-TAM crosstalk, significantly suppressing tumor proliferation and migration in both cellular and xenograft models. Notably, PB NPs exhibited excellent biocompatibility and showed no signs of hepatorenal toxicity in murine models, highlighting their translational potential for localized OSCC therapy.

This finding aligns with recent studies highlighting the multifaceted applications of PB NPs in cancer immunotherapy.[42] For example, Hou et al reported that iron ions released from PB NPs activate the IRF5 signaling pathway, thereby promoting M1 polarization of tumor-associated macrophages (TAMs).[26] Lian et al further demonstrated that engineered PB NPs

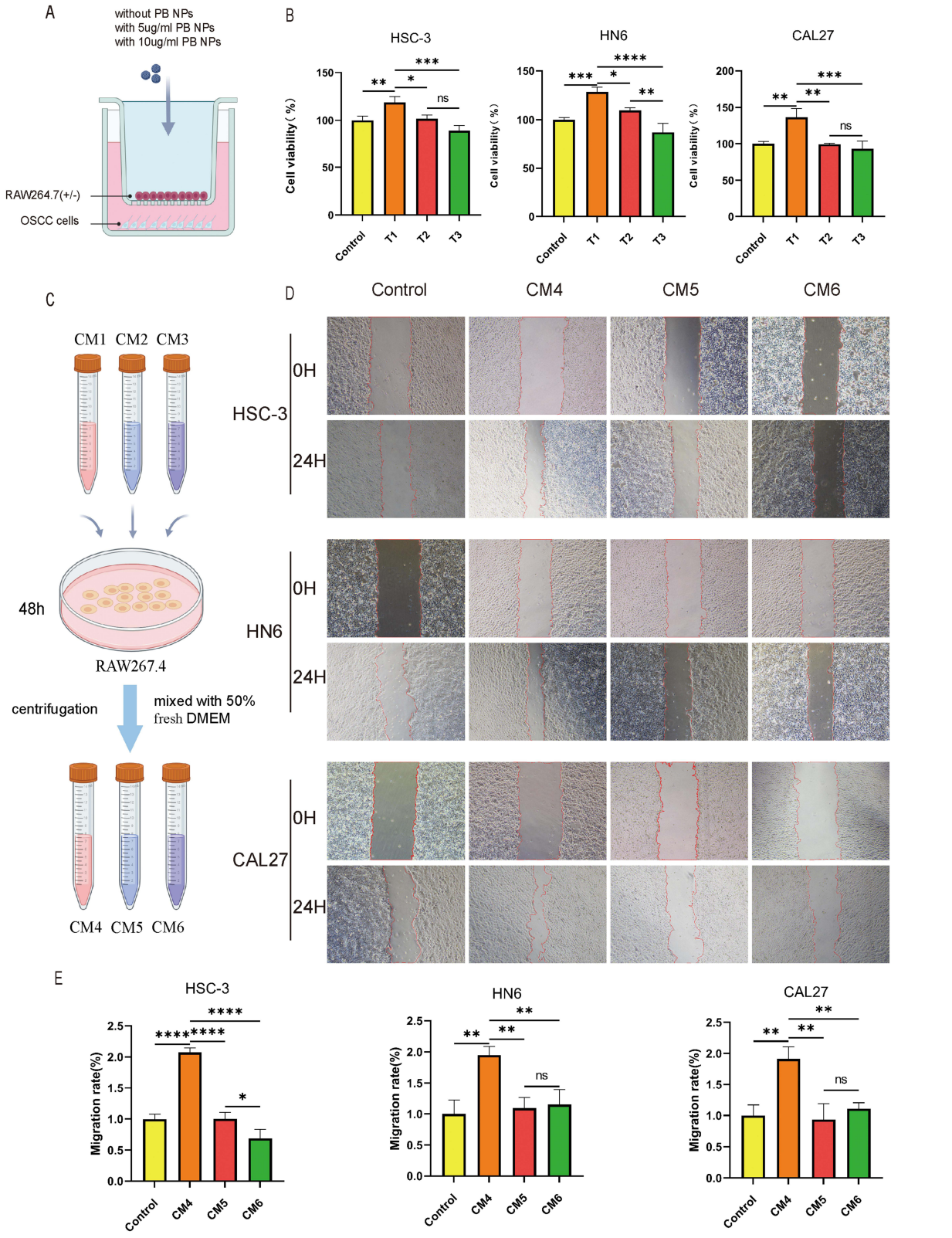

Figure 4 PB NPs disrupt the communication between OSCC and TAMs. (**A**) Schematic illustration of the coculture system. (**B**) Effect of different concentrations of PB NPs on OSCC cell proliferation. (**C**) Schematic representation of the preparation process for CM4, CM5, and CM6. (**D**) Effect of CM4, CD5, and CM6 on the migration ability of OSCC cells. (**E**) Migration rate of OSCC cells treated with CM4, CM5, and CM6.

Note: *p < 0.05, **p < 0.01, ***p < 0.001, ****p < 0.0001; "ns" indicates no significant difference.

https://doi.org/10.2147/IJN.S528763

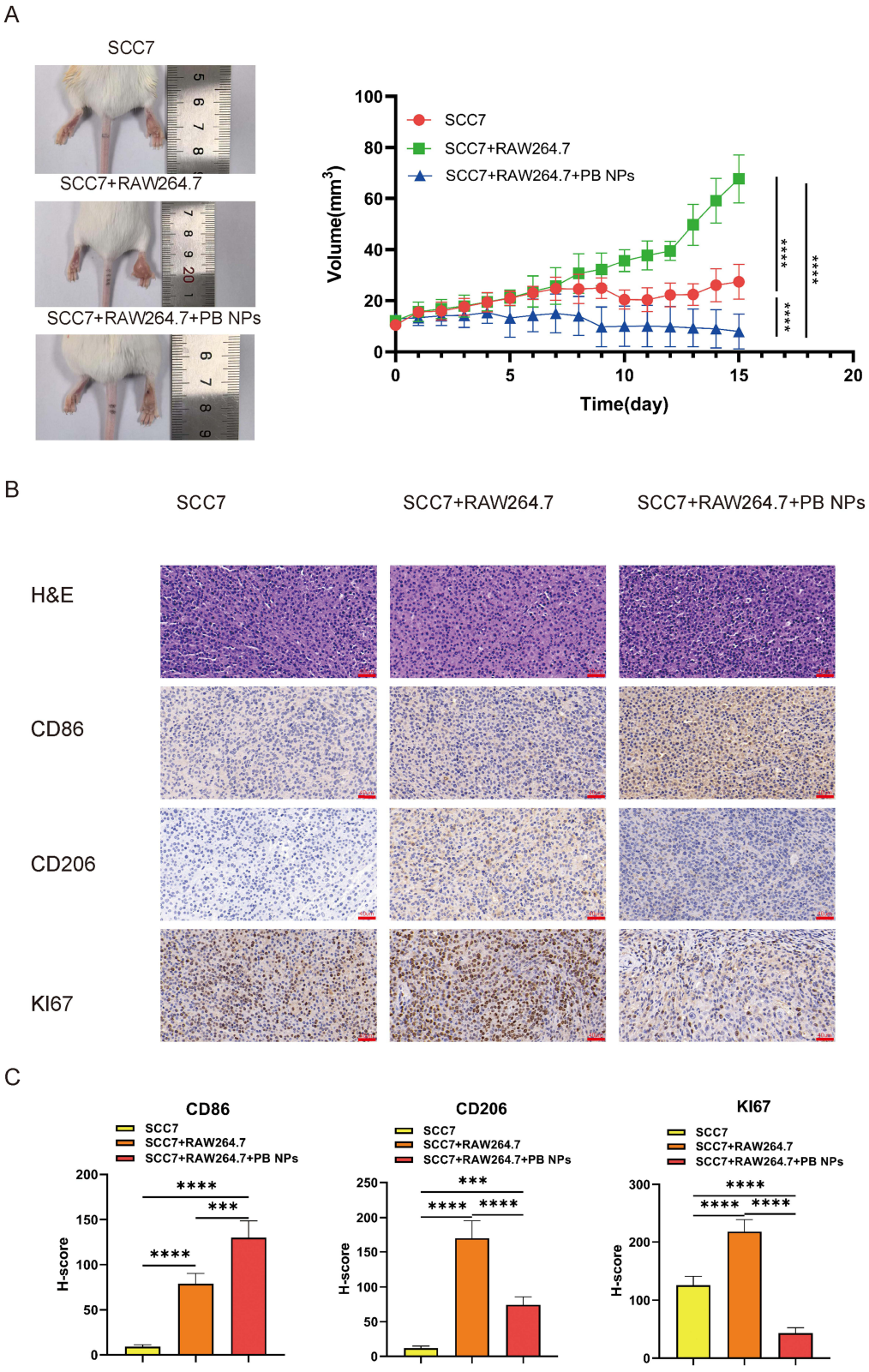

Figure 5 PB NPs influence the polarization of TAMs and proliferation of tumor cells in vivo.(**A**) Tumor volume measurements before and after treatment with PB NPs. (**B**) H&E and IHC staining of tumor tissues before and after treatment with PB NPs. Scale bars: 40 μm,(final magnification: ×800). (**C**) H-score of CD86, CD206, and KI67 in tumor tissues before and after treatment with PB NPs.
Note: ***p < 0.001, ****p < 0.0001.

effectively induce TAMs to adopt an M1-like phenotype by disrupting tumor glucose metabolism.[31] In this study, the therapeutic efficacy of PB NPs was further validated through functional experiments in the OSCC model. We observed that PB NP-induced macrophage polarization disrupted the interaction between OSCC cells and tumor-associated macrophages (TAMs), leading to a significant suppression of OSCC proliferation and migration in both cell co-culture systems and xenograft models.

Nanomaterials with immunomodulatory properties are emerging as powerful tools for remodeling the TME. Previous studies have shown that iron oxide nanoparticles induce M2-to-M1 polarization by activating the IRF5 signaling pathway,[43] while copper-selenium nanoparticles similarly promote M1 polarization, markedly inhibiting melanoma growth and recurrence.[44] Unlike these systems, which require complex surface modifications, PB NPs achieve TAM reprogramming through their intrinsic physicochemical properties—an advantage further reinforced by their FDA-approved clinical safety profile.

Building on these findings, we propose that localized peritumoral administration of PB NPs may synergize with existing immunotherapies. Recent preclinical studies have demonstrated that manganese-based nanoparticles significantly potentiate anti-PD1 therapy by synergistically targeting both innate and adaptive immunity.[45] Future research should explore similar combinatorial approaches, such as integrating PB NPs with anti-PD1 antibodies, to amplify antitumor immunity by concurrently targeting TAMs and T cells. However, persistent challenges—such as long-term polarization stability and systemic immune effects—must be addressed.

The physicochemical properties of nanomaterials, particularly their diameter and surface charge, play a critical role in modulating tumor progression by influencing tumor tissue permeability, cellular uptake efficiency, and biological toxicity. For example, smaller nanoparticles exhibit enhanced penetration through abnormal tumor vasculature and the extracellular matrix (ECM), leading to improved intratumoral drug distribution and effective targeting of deep-seated tumor cells.[46] Nanoparticles with low negative surface charge tend to display higher cytotoxicity, whereas positively charged nanoparticles, although less toxic, can enhance tumor cell killing through increased specificity and targeted delivery.[47] Overall, reducing particle size and incorporating a positive surface charge are commonly employed strategies to optimize antitumor efficacy. In this study, the diameter of the synthesized PB NPs exhibited was 57.43 ± 22.25 nm while the zeta potential was −17.36mV. Previous studies have demonstrated the successful synthesis of PB NPs with sizes below 10 nm. These findings suggest that future optimization of PB NP physicochemical properties may further enhance their inhibitory effects on OSCC.

Conclusion

In conclusion, this study demonstrated that PB NPs effectively reprogram TAMs within the OSCC microenvironment from the pro-tumorigenic M2 phenotype to the tumor-suppressive M1 phenotype, leading to significant antitumor effects. We successfully synthesized and characterized biocompatible PB NPs, confirmed their safety profile both in vitro and in vivo, and crucially, established their capacity to induce M1 polarization in TAMs, as evidenced by altered marker expression (increased CD86, decreased CD206) and cytokine secretion profiles (elevated TNF-α/IL-6, reduced TGF-β1). Furthermore, PB NPs disrupted the protumorigenic crosstalk between TAMs and OSCC cells, significantly inhibiting cancer cell proliferation and migration in vitro. These findings were robustly validated in an OSCC xenograft model, where peritumoral PB NP administration markedly suppressed tumor growth promoted by TAM co-inoculation, concurrently inducing a shift in intratumoral macrophage polarization towards M1 and reducing tumor cell proliferation. Collectively, our results establish PB NPs as a potent modulator of the immunosuppressive OSCC TME through targeted TAM reprogramming, offering a novel and promising immunotherapeutic strategy.

Acknowledgments

This work was supported by the National Natural Science Foundation of China (62375138/82403466) and the Nanjing Department of Health (YKK22177).

Disclosure

The authors report no conflicts of interest in this work.

References

1. Tan Y, Wang Z, Xu M, et al. Oral squamous cell carcinomas: state of the field and emerging directions. *Int J Oral Sci*. 2023;15(1):44. doi:10.1038/s41368-023-00249-w
2. Shang Q, Jiang Y, Wan Z, et al. The clinical implication and translational research of OSCC differentiation. *Br J Cancer*. 2024;130(4):660–670. doi:10.1038/s41416-023-02566-7
3. Romano A, Stasio DD, Petruzzi M, et al. Noninvasive imaging methods to improve the diagnosis of oral carcinoma and its precursors: state of the art and proposal of a three-step diagnostic process. *Cancers*. 2021;13(12):2864. doi:10.3390/cancers13122864
4. Chen L, Kong Q, Tian M, Zhang Q, Xia C, Deng C. Zn0.4Mg0.6Fe2O4 nanoenzyme: a novel chemo-sensitizer for the chemotherapy treatment of oral squamous cell carcinoma. *Nanoscale Adv*. 2023;5(3):851. doi:10.1039/d2na00750a
5. Huang Y, Sun J, Li J, et al. Neoadjuvant Immunochemotherapy for locally advanced resectable oral squamous cell carcinoma: a prospective single-arm trial (illuminate trial). *Int J Surg*. 2023;109(8):2220–2227. doi:10.1097/JS9.0000000000000489
6. Radaic A, Kamarajan P, Cho A, et al. Biological biomarkers of oral cancer. *Periodontol 2000*. 2024;96(1):250–280. doi:10.1111/prd.12542
7. Jiménez-Labaig P, Rullan A, Hernando-Calvo A, et al. A systematic review of antibody-drug conjugates and bispecific antibodies in head and neck squamous cell carcinoma and nasopharyngeal carcinoma: charting the course of future therapies. *Cancer Treat Rev*. 2024;128:102772. doi:10.1016/j.ctrv.2024.102772
8. Zhu J, Lu H, Wang K, Liu B, Yan J. Tertiary lymphoid structures in head and neck squamous cell carcinoma. *Transl Oncol*. 2024;44:101949. doi:10.1016/j.tranon.2024.101949
9. Wang G, Zhang M, Cheng M, et al. Tumor microenvironment in head and neck squamous cell carcinoma: functions and regulatory mechanisms. *Cancer Lett*. 2021;507:55–69. doi:10.1016/j.canlet.2021.03.009
10. Du M, Sun L, Guo J, Lv H. Macrophages and Tumor-Associated Macrophages in the Senescent Microenvironment: from Immunosuppressive TME to Targeted Tumor Therapy. *Pharmacol Res*. 2024;204:107198. doi:10.1016/j.phrs.2024.107198
11. Wang Z, Kirkwood KL, Wang Y, et al. Analysis of the effect of CCR7 on the microenvironment of mouse oral squamous cell carcinoma by single-cell RNA sequencing technology. *J Exp Clin Cancer Res*. 2024;43:94. doi:10.1186/s13046-024-03013-y
12. Li QL, Mao J, Meng XY. Comprehensive characterization of immune landscape based on tumor microenvironment for oral squamous cell carcinoma prognosis. *Vaccines*. 2022;10(9):1521. doi:10.3390/vaccines10091521
13. Sales de Sá R, Miranda Galvis M, Mariz BALA, et al. Increased tumor immune microenvironment cd3+ and cd20+ lymphocytes predict a better prognosis in oral tongue squamous cell carcinoma. *Front Cell Dev Biol*. 2021;8:622161. doi:10.3389/fcell.2020.622161
14. Qin Y, Zheng X, Gao W, Wang B, Wu Y. Tumor microenvironment and immune-related therapies of head and neck squamous cell carcinoma. *Mol Ther Oncolytics*. 2021;20:342. doi:10.1016/j.omto.2021.01.011
15. Ocaña MC, Martínez-Poveda B, Quesada AR, Medina MÁ. Metabolism within the tumor microenvironment and its implication on cancer progression: an ongoing therapeutic target. *Med Res Rev*. 2019;39(1):70–113. doi:10.1002/med.21511
16. Yang L, Lin PC. Mechanisms that drive inflammatory tumor microenvironment, tumor heterogeneity, and metastatic progression. *Semin Cancer Biol*. 2017;47:185–195. doi:10.1016/j.semcancer.2017.08.001
17. El Alaa RSA, Al-Mannai W, Darwish N, Al-Mansoori L. Adipose-derived stromal cells and cancer-associated fibroblasts: interactions and implications in tumor progression. *Int J Mol Sci*. 2024;25(21):11558. doi:10.3390/ijms252111558
18. Liu T, Guo S, Ji Y, Zhu W. Role of cancer-educated mesenchymal stromal cells on tumor progression. *Biomed Pharmacother*. 2023;166:115405. doi:10.1016/j.biopha.2023.115405
19. Huang T, Song X, Xu D, et al. Stem Cell programs in cancer initiation, progression, and therapy resistance. *Theranostics*. 2020;10(19):8721–8743. doi:10.7150/thno.41648
20. Alves A, Diel L, Ramos G, et al. Tumor microenvironment and oral squamous cell carcinoma: a crosstalk between the inflammatory state and tumor cell migration. *Oral Oncol*. 2021;112:105038. doi:10.1016/j.oraloncology.2020.105038
21. Liu Y, Liang J, Zhang Y, Guo Q. Drug resistance and tumor immune microenvironment: an overview of current understandings (Review). *Int J Oncol*. 2024;65(4):96. doi:10.3892/ijo.2024.5684
22. Wang X, Wang J, Zhao J, Wang H, Chen J, Wu J. HMGA2 facilitates colorectal cancer progression via STAT3-mediated tumor-associated macrophage recruitment. *Theranostics*. 2022;12(2):963–975. doi:10.7150/thno.65411
23. Boutilier AJ, Elsawa SF. macrophage polarization states in the tumor microenvironment. *Int J Mol Sci*. 2021;22(13):6995. doi:10.3390/ijms22136995
24. Kerneur C, Cano CE, Olive D. Major pathways involved in macrophage polarization in cancer. *Front Immunol*. 2022;13:1026954. doi:10.3389/fimmu.2022.1026954
25. Saeedifar AM, Mosayebi G, Ghazavi A, Bushehri RH, Ganji A. Macrophage polarization by phytotherapy in the tumor microenvironment. *Phytother Res*. 2021;35(7):3632–3648. doi:10.1002/ptr.7058
26. Hou L, Gong X, Yang J, Zhang H, Yang W, Chen X. Hybrid-membrane-decorated prussian blue for effective cancer immunotherapy via tumor-associated macrophages polarization and hypoxia relief. *Adv. Mater.* 2022;34(14):2200389. doi:10.1002/adma.202200389
27. Su YY, Jiang XY, Zheng LJ, et al. Hybrid au-star@prussian blue for high-performance towards bimodal imaging and photothermal treatment. *J Colloid Interface Sci*. 2023;634:601–609. doi:10.1016/j.jcis.2022.12.043
28. Wang Y, Liang Z, Liang Z, Lv W, Chen M, Zhao Y. Advancements of prussian blue-based nanoplatforms in biomedical fields: progress and perspectives. *J Control Release*. 2022;351:752–778. doi:10.1016/j.jconrel.2022.10.007
29. Chen S, Luo X, Ma R, et al. Promotes M1-polarization and diabetic wound healing using prussian blue nanozymes. *Int immunopharmacol*. 2024;141:113009. doi:10.1016/j.intimp.2024.113009
30. Leftin A, Koutcher JA. Quantification of nanoparticle enhancement in polarized breast tumor macrophage deposits by spatial analysis of MRI and histological iron contrast using computer vision. *Contrast Media Mol Imaging*. 2018;2018:3526438. doi:10.1155/2018/3526438
31. Yang Y, Liu Q, Wang M, et al. Genetically programmable cell membrane-camouflaged nanoparticles for targeted combination therapy of colorectal cancer. *Signal Transduct Target Ther*. 2024;9(1):158. doi:10.1038/s41392-024-01859-4
32. Pelaez-Prestel HF, Gonzalez-Martin F, Ras-Carmona A, et al. Oral squamous cell carcinomas drive monocytes into immunosuppressive CD25+CD163+CD206+ macrophages. *Oral Oncol*. 2024;159:107078. doi:10.1016/j.oraloncology.2024.107078

33. Qin Z, Li X, Wang P, et al. Ultrasmall prussian blue nanozyme attenuates osteoarthritis by scavenging reactive oxygen species and regulating macrophage phenotype. *Nano Lett*. 2024;24(37):11697–11705. doi:10.1021/acs.nanolett.4c03314
34. *Uncovering the Fate and Risks of Intravenously Injected Prussian Blue Nanoparticles in mice by an Integrated Methodology of Toxicology, Pharmacokinetics, Proteomics, and Metabolomics - PubMed*. Available from: https://pubmed.ncbi.nlm.nih.gov/37147710/. Accessed June 26, 2025.
35. Almarshad HA, Elderdery A, Alenazy FO, Elissidig SA. Impact of gold nanoparticles intraperitoneal injection on mice's erythrocytes and renal tissue. *IEEE Trans NanoBiosci*. 2025;24(2):174–179. doi:10.1109/TNB.2024.3471813
36. Xia C, Pan J, Wang J, et al. Functional blockade of cancer-associated fibroblasts with ultrafine gold nanomaterials causes an unprecedented bystander antitumoral effect. *Nanoscale*. 2020;12(38):19833–19843. doi:10.1039/D0NR04682E
37. Xiang T, Li H, Wang X, Su D. Melanocortin-1 receptor expression as a predictive factor for postoperative outcomes in melanoma patients: a retrospective study. *Front Immunol*. 2025;16:1570502. doi:10.3389/fimmu.2025.1570502
38. Zhang Q, Sioud M. Tumor-associated macrophage subsets: shaping polarization and targeting. *Int J Mol Sci*. 2023;24(8):7493. doi:10.3390/ijms24087493
39. Vitale I, Manic G, Coussens LM, Kroemer G, Galluzzi L. Macrophages and metabolism in the tumor microenvironment. *Cell Metab*. 2019;30(1):36–50. doi:10.1016/j.cmet.2019.06.001
40. Xiang X, Wang J, Lu D, Xu X. Targeting tumor-associated macrophages to synergize tumor immunotherapy. *Signal Transduct Target Ther*. 2021;6:75. doi:10.1038/s41392-021-00484-9
41. Martori C, Sanchez-Moral L, Paul T, et al. Macrophages as a therapeutic target in metastatic prostate cancer: a way to overcome immunotherapy resistance? *Cancers*. 2022;14(2):440. doi:10.3390/cancers14020440
42. Zhang J, Wang F, Sun Z, Ye J, Chu H. Multidimensional applications of prussian blue-based nanoparticles in cancer immunotherapy. *J Nanobiotechnol*. 2025;23(1):161. doi:10.1186/s12951-025-03236-x
43. Li Y, Li M, Zheng J, et al. Ultrasound-responsive nanocarriers delivering siRNA and Fe3O4 nanoparticles reprogram macrophages and inhibit m2 polarization for enhanced nsclc immunotherapy. *ACS Appl Mater Interfaces*. 2024;16(42):56634–56652. doi:10.1021/acsami.4c10036
44. Zheng Y, Han Y, Wang T, et al. Reprogramming tumor-associated macrophages via ROS-mediated novel mechanism of ultra-small cu2−se nanoparticles to enhance anti-tumor immunity. *Adv Funct Mater*. 2022;32(12):2108971. doi:10.1002/adfm.202108971
45. Geng Z, Chen F, Wang X, Wang L, Pang Y, Liu J. Combining Anti-PD-1 antibodies with Mn2+-Drug Coordinated multifunctional nanoparticles for enhanced cancer therapy. *Biomaterials*. 2021;275:120897. doi:10.1016/j.biomaterials.2021.120897
46. Nekoueifard E, Radmanesh F, Zarkesh I, et al. Switchable PAMAM megamers for deep tumor penetration and enhanced cell uptake. *J Control Release*. 2024;375:478–494. doi:10.1016/j.jconrel.2024.09.031
47. Dependence of Quantum Dot Toxicity In Vitro on Their Size, Chemical Composition, and Surface Charge - PubMed. Available from: https://pubmed.ncbi.nlm.nih.gov/36014600/. Accessed June 26, 2025.